

# UCSF

## UC San Francisco Previously Published Works

### Title

Broad Distribution of Hepatocyte Proliferation in Liver Homeostasis and Regeneration

### Permalink

<https://escholarship.org/uc/item/0f93z7p7>

### Journal

Cell Stem Cell, 26(1)

### ISSN

1934-5909

### Authors

Chen, Feng  
Jimenez, Robert J  
Sharma, Khushbu  
[et al.](#)

### Publication Date

2020

### DOI

10.1016/j.stem.2019.11.001

Peer reviewed



# HHS Public Access

Author manuscript

*Cell Stem Cell*. Author manuscript; available in PMC 2021 March 30.

Published in final edited form as:

*Cell Stem Cell*. 2020 January 02; 26(1): 27–33.e4. doi:10.1016/j.stem.2019.11.001.

## Broad Distribution of Hepatocyte Proliferation in Liver Homeostasis and Regeneration

Feng Chen<sup>1,\*</sup>, Robert J. Jimenez<sup>1</sup>, Khushbu Sharma<sup>1,2</sup>, Hubert Y. Luu<sup>1,3</sup>, Bernadette Y. Hsu<sup>1,4</sup>, Ajay Ravindranathan<sup>5</sup>, Bradley A. Stohr<sup>5</sup>, Holger Willenbring<sup>1,6,7,8,\*</sup>

<sup>1</sup>Eli and Edythe Broad Center of Regeneration Medicine and Stem Cell Research, University of California, San Francisco, San Francisco, CA 94143, USA

<sup>2</sup>College of Arts and Sciences, University of San Francisco, San Francisco, CA 94117, USA

<sup>3</sup>Division of General Surgery, Department of Surgery, University of California, San Francisco, San Francisco, CA 94143, USA

<sup>4</sup>Biomedical Sciences Graduate Program, University of California, San Francisco, San Francisco, CA 94143, USA

<sup>5</sup>Division of Surgical Pathology, Department of Pathology, University of California, San Francisco, San Francisco, CA 94143, USA

<sup>6</sup>Division of Transplant Surgery, Department of Surgery, University of California, San Francisco, San Francisco, CA 94143, USA

<sup>7</sup>Liver Center, University of California, San Francisco, San Francisco, CA 94143, USA

<sup>8</sup>Lead Contact

### SUMMARY

Hepatocyte proliferation is the principal mechanism for generating new hepatocytes in liver homeostasis and regeneration. Recent studies have suggested that this ability is not equally distributed among hepatocytes but concentrated in a small subset of hepatocytes acting like stem cells, located around the central vein or distributed throughout the liver lobule and exhibiting active WNT signaling or high telomerase activity, respectively. These findings were obtained by utilizing components of these growth regulators as markers for genetic lineage tracing. Here, we used random lineage tracing to localize and quantify clonal expansion of hepatocytes in normal and injured liver. We found that modest proliferation of hepatocytes distributed throughout the lobule maintains the hepatocyte mass and that most hepatocytes proliferate to regenerate it, with

\*Correspondence: feng.chen@ucsf.edu (F.C.), holger.willenbring@ucsf.edu (H.W.).

#### AUTHOR CONTRIBUTIONS

F.C. and H.W. conceived and designed the experiments. F.C., R.J.J., K.S., H.Y.L., B.Y.H., and A.R. performed and analyzed the experiments. B.A.S. provided reagents.

#### DECLARATION OF INTERESTS

H.W. is co-founder and advisory board member of Ambys Medicines. The authors declare no competing interests.

#### DATA AND CODE AVAILABILITY

This study did not generate/analyze datasets/code.

#### SUPPLEMENTAL INFORMATION

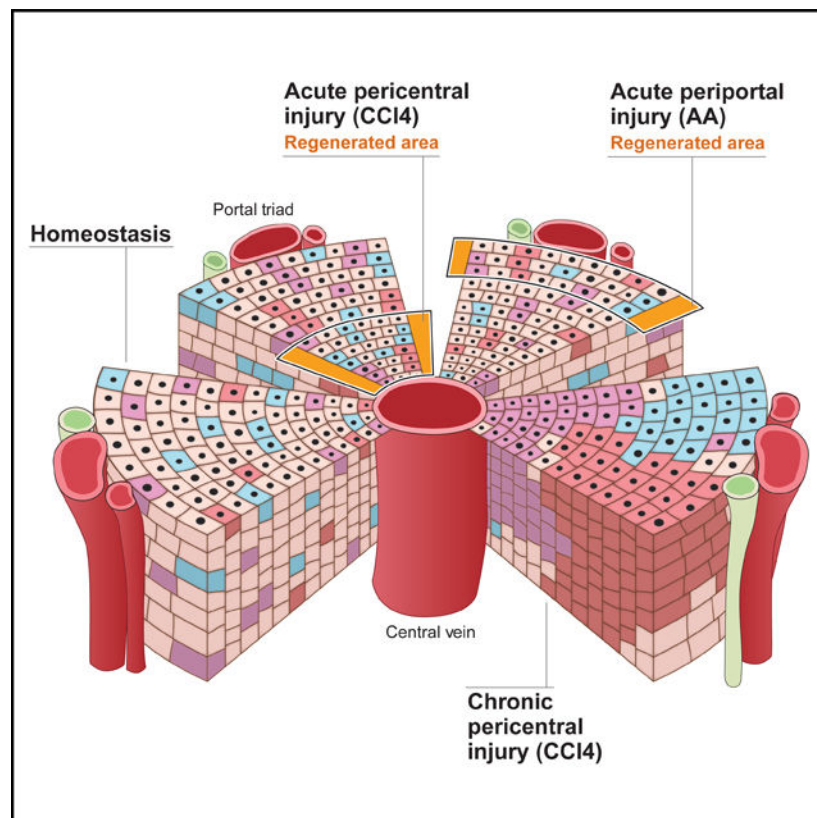
Supplemental Information can be found online at <https://doi.org/10.1016/j.stem.2019.11.001>.

diploidy providing a growth advantage over polyploidy. These results show that the ability to proliferate is broadly distributed among hepatocytes rather than limited to a rare stem cell-like population.

## In Brief

Chen et al. investigate potential differences in how much hepatocytes in the different zones of the liver lobule contribute to hepatocyte replacement in normal and injured liver. They find that, in principle, location and extent of hepatocyte proliferation are broadly distributed, with specific effects of type of injury and ploidy.

## Graphical abstract



## INTRODUCTION

Hepatocytes are unique among differentiated cells because they provide many vital functions and also can proliferate extensively, which allows efficient liver regeneration after injury. It is increasingly appreciated that hepatocytes are a heterogeneous cell population—depending on where they are located in the liver lobule, hepatocytes have different functions; they also differ in ploidy. Recently, hepatocyte heterogeneity was shown to extend to proliferation. In the normal liver, hepatocytes bordering on the central vein were found to harness WNT signaling to proliferate more than other hepatocytes, making them the main source of new hepatocytes (Wang et al., 2015). Another study showed that rare hepatocytes with high

telomerase activity distributed throughout the liver lobule dominate both liver homeostasis and regeneration (Lin et al., 2018).

These findings suggest that the hepatocyte mass is maintained and restored by clonal expansion of a small subset of hepatocytes acting like stem cells. However, it is currently not known which of the 2 hepatocyte stem cell models is correct or if both are, and the relative contribution of other hepatocytes to liver homeostasis and regeneration has not been addressed. In addition, these findings were obtained using lineage tracing disrupting endogenous *Axin2* or *Tert* genes, potentially altering how readily and extensively cells respond to growth signals (Minear et al., 2010; Sarin et al., 2005).

## RESULTS

To address these questions, we used random lineage tracing—capturing a representative sample of all hepatocytes—to localize and quantify their clonal expansion in normal and injured liver. We permanently labeled hepatocytes throughout the liver lobule at a neutral genetic locus with 1 of 3 fluorophores by intravenously injecting AAV8-TBG-Cre into adult heterozygous Rosa26-Rainbow Cre reporter (*R26<sup>R<sup>rb</sup>/wt</sup>*) mice (Figure 1A); the mice were housed under standard barrier conditions and any health problems were recorded (Table S1). Lineage tracing was active by 2 weeks after vector injection (Figures 1B and S1A). As previously reported for adeno-associated virus (AAV) capsids (Davidoff et al., 2003), including the AAV8 capsid (Greig et al., 2018), the labeling efficiency was higher in males than females and varied with weight (data not shown). Therefore, we doubled the dose in females and adjusted it to each mouse's weight (Table S1). We used decreasing vector doses to induce high-, medium-, and low-density lineage tracing (Figure S1A; Table S1). The labeling efficiency gradually decreased along the central to portal axis, a characteristic of the AAV8 capsid (Bell et al., 2011; Figures 1B, S1A, and S1B). We used heterozygous mice to distinguish diploid from polyploid hepatocytes based on expression of 1 or 2 fluorophores, respectively. Accordingly, we found that lineage-traced hepatocytes expressing only 1 fluorophore were enriched for mononucleated cells, whereas those expressing 2 were enriched for binucleated cells (Figure S1C).

We started our investigation of hepatocyte proliferation in the normal liver by analyzing 2D clusters in mice after long-term lineage tracing. We found no or only modest expansion of labeled hepatocytes 9.5–17 months after AAV vector injection; we did not see large clusters or hepatocytes that streamed across the lobule (Figures 1C–1E). Moreover, the distribution of labeled hepatocytes appeared similar to that at 2 weeks after AAV vector injection, with denser labeling in the pericentral zone of the lobule (Figures 1B, S1A, and S1B). Had pericentral hepatocytes replenished the midlobular and periportal zones with new hepatocytes, the density of labeled cells in these zones should have increased.

Because 2D imaging of hepatocyte clusters might omit cells that lie beyond the plane of the section, we imaged 3D hepatocyte clones by confocal microscopy of liver tissue cleared using a modified CUBIC protocol (Susaki et al., 2015). This approach allowed us to image up to 150  $\mu\text{m}$  deep through several hepatocyte layers, which confirmed absence of large

clones or streaming of hepatocytes 13.5 or 17 months after injection of high (Video S1A) or medium (data not shown) AAV vector doses.

Next, we focused on the mice that received the low AAV vector dose. 2 to 3 weeks after injection, virtually all (457/467) labeled hepatocytes were single cells (Figure 1F; Video S1B). We rarely saw 2 differently colored clones next to each other (Figure S1D) and almost never 2 adjacent clones sharing a border (Video S1B). Few (10/467) clones that consisted of 2 cells expressing the same fluorophore were likely hepatocytes that proliferated between the time of AAV vector injection and analysis because they share a substantial cell border (Figure S1D) and because the probability of 2 different clones expressing the same fluorophore is only 1/3 or even less if cells are polyploid. Therefore, we used the mice that received the low AAV vector dose to quantify the size of individual clones.

We did not find large clones or streaming of hepatocytes 9.5–15 months after AAV vector injection when we imaged 5–23 fields (each containing at least 1 portal vein and 1 central vein and ~1,600 hepatocytes) from each of the left, median, right anterior, and right posterior lobe or the median or left lobe of each mouse (Videos S1C and S1D; Table S1). Specific analysis of 458 clones from at least 1 field per mouse at 9.5–9.7 months showed that 84.1% of hepatocytes did not proliferate but remained single cells, 14.0% of hepatocytes divided once and gave rise to 2-cell clones, and 1.7% gave rise to 3-to 4-cell clones; only 1 (0.2%) clone was larger, consisting of 6 cells. Similarly, of 978 clones analyzed in mice at 13.6–13.7 months, 90.1% were single cells, 9.0% were 2-cell clones, 0.7% were 3-to 4-cell clones, and 0.2% consisted of 5–7 cells (Figure 1F; Videos S1C–S1E). Clones >2 cells were mostly located in the midlobular zone; pericentral and periportal clones almost exclusively consisted of 1 or 2 cells (Figure 1F). Hepatocytes proliferated more in females than in males, particularly in the midlobular zone, which was associated with higher baseline levels of CCND1 (Alvarado et al., 2016; Figures S1E–S1I). Clones >4 cells expressed only 1 fluorophore but at <1% were too rare to establish a growth advantage of diploid hepatocytes (Figure S1J). In accord, overall clonal expansion followed a Poisson distribution (Figure S1K), suggesting that hepatocyte proliferation occurs randomly in liver homeostasis.

To exclude that AAV vector transduction affected hepatocyte proliferation, we devised a lineage tracing strategy that let us compare the proliferation of transduced and untransduced cells. We intravenously co-injected adult Cre and Flp double-reporter (*R26R<sup>tdRFP/ZG</sup>*) mice with AAV8-TBG-Cre and AAV9-TTR-Flp at doses that activate Cre-dependent tdRFP in all but a few sparsely distributed hepatocytes and Flp-dependent EGFP in a small fraction of hepatocytes (Figures 1G and S1L; Table S1). Because Cre- and Flp-mediated reporter activation is very efficient in the normal liver (Schaub et al., 2018; Yanger et al., 2014), hepatocytes negative for both tdRFP and EGFP can be assumed to not have been transduced with either AAV vector. When we examined the number of hepatocytes in individual 2D clusters 2 weeks and 9.7 months after AAV injection, we found that hepatocytes not transduced with AAV vectors and hepatocytes labeled by AAV9-TTR-Flp expanded similarly at the 2 time points (Figures 1H and S1M), demonstrating that AAV transduction did not affect hepatocyte proliferation. Further analysis of the untransduced clusters confirmed our initial finding of modest hepatocyte proliferation in all 3 zones, with more

proliferation occurring in the midlobular zone, and absence of streaming of hepatocytes (Figures 1I and S1N).

We also investigated clonal expansion of hepatocytes in the injured liver. After intravenously injecting low-or high-dose AAV8-TBG-Cre into adult *R26<sup>Rb/wt</sup>* mice, we specifically injured their pericentral or periportal hepatocytes by intraperitoneal injection of 1 dose of carbon tetrachloride (CCl<sub>4</sub>) or 2 doses of allyl alcohol (AA), respectively (Figures S2A and S2B). We found that these acute injuries—depleting ~1/2 or ~1/4 of the hepatocyte mass, respectively—induced proliferation of hepatocytes adjacent to the injured area, leading to mostly 2-to 3-cell clones extending into the necrotic area (Figures 2A, 2B, and 2D). In addition to this localized repair, we saw compensatory proliferation of hepatocytes in zones further away from the injury (Figures 2A, 2B, 2D, S2C, and S2D).

Next, we modeled chronic liver injury by repeating CCl<sub>4</sub> application as soon as hepatocyte regeneration was complete (Figures S2E and S2F). After 3 doses of CCl<sub>4</sub>, we found that  $84.9\% \pm 2.2\%$  of lineage-traced hepatocytes in all zones divided, with  $65.9\% \pm 2.2\%$  dividing at least twice, giving rise to clones consisting of 3 cells (Figures 2C and 2D; Video S1F). Hepatocyte proliferation was similar between males and females and uniform across the lobule (Figures 2C and 2D). Clone morphology ranged from single enlarged cells—characteristic of hepatocyte hypertrophy, as after partial hepatectomy (Miyaoaka et al., 2012)—to clones consisting of several small cells that streamed along the portal to central axis or formed nodules (Figure 2E; Video S1F). Although many 1-cell clones were enlarged after either chronic or acute injury ( $54.6\% \pm 2.0\%$  of 69–102 clones each in 2 males and 2 females for  $3 \times$  CCl<sub>4</sub>,  $28.0\% \pm 2.0\%$  of 25–30 clones each in 1 male and 2 females for  $1 \times$  CCl<sub>4</sub>, and  $35.2\% \pm 4.7\%$  of 32–48 clones each in 2 males and 1 female for AA), proliferation was the predominant mechanism of hepatocyte regeneration (Figure 2D).

Applying additional CCl<sub>4</sub> doses promoted the expansion of hepatocyte clones throughout the lobule. After 6 doses of CCl<sub>4</sub>, we found large clones (~7 cells in 2D) in the periportal and midlobular zones that converged to form regenerative patches (Figures 2C and S2G). Most hepatocytes in these clones were small, but large cells could also be found within a clone, suggesting that hepatocytes can switch from proliferation to hypertrophy (Figure 2F). After 12 doses of CCl<sub>4</sub>, we saw very large clones (~20 cells in 2D), some of which covered the distance from the portal vein to the central vein (Figures 2C, 2G, and S2H). In addition, we saw large clones in the midlobular zone, both right next to and further away from the pericentral zone (Figure S2H; Video S1G). 1-or 2-cell clones were rare but could still be found; the cells were large and elongated (Figure 2G). However, most lineage-traced hepatocytes divided markedly after 6 or 12 doses of CCl<sub>4</sub> (Figures 2C, 2G, S2G, and S2H).

Diploid hepatocytes proliferated more efficiently than polyploid hepatocytes—in normal liver, most ( $69.4\% \pm 10.3\%$ ) clones, independent of size or location, were polyploid, whereas after 12 doses of CCl<sub>4</sub>, most ( $71.9\% \pm 7.0\%$ ) large clones were diploid (Figures 2H and 2I).

## DISCUSSION

In summary, our random lineage tracing of hepatocytes in the normal liver does not show predominant proliferation of pericentral hepatocytes, leading to large hepatocyte patches streaming toward the periportal zone, as was shown by lineage tracing of *Axin2*-expressing hepatocytes (Wang et al., 2015). We did not find that the dose of tamoxifen used for *Axin2* lineage tracing significantly induces clonal expansion of hepatocytes (Figure S2I), suggesting genetic or environmental differences, e.g., *Axin2* haploinsufficiency or diet and housing, as potential reasons for the discrepant results. In accord with results from lineage tracing of hepatocytes exhibiting high *Tert* expression (Lin et al., 2018), we found that hepatocyte proliferation occurs throughout the liver lobule, with a slight predominance of the midlobular zone. Our results differ in how much each lineage-traced hepatocyte proliferates: high-*Tert* lineage tracing showed an average clone size of 4.2 cells at 6 months, with 64% of clones being >2 cells; expansion of lineage-traced hepatocytes from 3%–5% to 30% suggests an average clone size of 6–10 cells at 1 year (Lin et al., 2018). We found an average clone size of 1.1 cells at 13.6–13.7 months, with 9.9% of lineage-traced hepatocytes proliferating and 0.9% of clones being >2 cells (average clone size of 3.9 cells). To confirm that our strategy captured a representative sample of all hepatocytes, we ascertained that it was not biased against cells highly expressing *Tert* or *Axin2* (Figures S2J–S2N). Our results show that modest proliferation of hepatocytes in all zones maintains the hepatocyte mass, which is consistent with most hepatocytes being long lived as suggested by isotope labeling (Arrojo E Drigo et al., 2019).

Our findings were similar for how the hepatocyte mass is restored in the injured liver. Acute loss of pericentral or periportal hepatocytes is repaired by proliferation of adjacent hepatocytes, aided by proliferation of hepatocytes located further away from the injury. Repeated pericentral injury leads to clonal expansion of as many as 85% of hepatocytes in all zones. As clones derived from midlobular hepatocytes moving into the pericentral injury zone continue to be depleted, periportal hepatocytes give rise to large clones that stream along the portal to central axis (Font-Burgada et al., 2015). Although diploidy does not have a significant effect on hepatocyte proliferation in the normal liver, it affords a selective growth advantage in the chronically injured liver (Wilkinson et al., 2019). Diploid clones may derive from pre-existing diploid hepatocytes or form by ploidy reversal of polyploid hepatocytes (Duncan et al., 2010).

Collectively, our findings show that the ability to proliferate is not concentrated in rare stem cell-like hepatocytes but distributed among hepatocytes in liver homeostasis and regeneration, with type of injury and ploidy affecting location and extent of proliferation. Because hepatocytes are constantly exposed to exogenous and endogenous toxins, it is conceivable that this principle of broad distribution of proliferation evolved to reinforce regeneration and minimize cancer risk.

## STAR★METHODS

### LEAD CONTACT AND MATERIALS AVAILABILITY

Further information and requests for resources and reagents should be directed to and will be fulfilled by the Lead Contact, Holger Willenbring (holger.willenbring@ucsf.edu). This study did not generate new unique reagents.

### EXPERIMENTAL MODEL AND SUBJECT DETAILS

**Mice**—All mice were housed under standard barrier conditions and experiments were approved by the Institutional Animal Care and Use Committee at UCSF. Mice were bred in mating pairs as 1 male with 1 female, or trios of 1 male with 2 females. All mice were housed at ambient room temperature in groups of up to 5 mice; remaining males of each litter were housed singly. All mice were immune competent, not involved in previous procedures, and drug and test naive. Food (diets specified in Table S1) and water was provided ad libitum. *R26R<sup>tb/tb</sup>* mice (Red-Horse et al., 2010) (gift from Irving Weissman, Stanford University) maintained on a C57BL/6 background were bred to wild-type C57BL/6J mice (Jackson Laboratory, Stock# 000664) to generate *R26R<sup>tb/wt</sup>* mice. *R26R<sup>tdRFP/ZG</sup>* mice were generated by removing the Cre reporter from *R26R<sup>NZG/NZG</sup>* mice (Yamamoto et al., 2009) (Jackson Laboratory, Stock# 012429) as previously reported (Schaub et al., 2018), and crossing the resulting *R26R<sup>ZG/ZG</sup>* mice with *R26R<sup>tdRFP/tdRFP</sup>* mice (Luche et al., 2007). *R26R<sup>tdRFP/ZG</sup>* mice were maintained on a mixed C57BL/6 and FVB background.

### METHOD DETAILS

**AAV vector injection and dosing**—All AAV vectors were diluted in PBS with 5% sorbitol and 100  $\mu$ L were intravenously injected through the tail vein. For high, medium, and low-density lineage tracing, 8–15-week-old male or female *R26R<sup>tb/wt</sup>* mice were injected with AAV8-TBG-Cre at  $1.01 \times 10^9$  viral genomes per gram body weight (vg/g),  $3.35 \times 10^8$  vg/g, and  $5.58 \times 10^7$  vg/g or  $2.01 \times 10^9$  vg/g,  $6.70 \times 10^8$  vg/g, and  $1.12 \times 10^8$  vg/g, respectively. Liver tissue was collected for analysis 2–3 weeks after AAV vector injection, or mice were maintained for up to 17 months. Injury protocols were started 2–4 weeks after AAV vector injection. To induce dual labeling of hepatocytes, 12-week old male or female *R26R<sup>tdRFP/ZG</sup>* mice were injected with  $6.09 \times 10^9$  vg/g or  $1.00 \times 10^{10}$  vg/g AAV8-TBG-Cre and  $3.48 \times 10^8$  vg/g or  $4.00 \times 10^8$  vg/g AAV9-TTR-Flp, respectively. Liver tissue was collected for analysis 2 weeks after AAV vector injection, or mice were maintained for 9.7 months.

**Liver injury protocols**—CCl<sub>4</sub> was intraperitoneally injected as a 1:4 dilution with corn oil. A dose of 1  $\mu$ L/g body weight was used to induce acute pericentral injury. A dose of 0.5  $\mu$ L/g every 3–4 days for a total of 3, 6, or 12 doses was used to induce chronic injury. Liver tissue was collected for analysis 2 days, 3–6 days, or 2 weeks after the last dose. AA was intraperitoneally injected as a 1% solution with sodium chloride 0.9% to induce acute periportal injury. Mice received 0.030  $\mu$ L/g body weight followed 3 days later by 0.046  $\mu$ L/g (< 20 g), 0.060  $\mu$ L/g (20–30 g), or 0.076  $\mu$ L/g (30–40 g). Liver tissue was collected for analysis 1 day, 1 week, or 2 weeks after the last dose. Untreated controls were analyzed 2–3

weeks after AAV injection. Tamoxifen was intraperitoneally injected as a 20 mg/mL solution in corn oil at a dose of 160 µg/g body weight 2–3 weeks after AAV injection. Liver tissue was collected for analysis 4 weeks later. Untreated controls were analyzed 7 weeks after AAV injection. Protocols were established in C57BL/6 and mixed C57BL/6 and FVB mice.

**Tissue collection, processing and imaging**—Livers were perfused with 4% paraformaldehyde (PFA), cut into 0.5 cm-thick pieces, and further fixed in 4% PFA for 4–8 hours at 4°C (*R26R<sup>rb/wt</sup>* mice) or overnight (all other mice). Tissues for paraffin embedding were fixed overnight in 10% formalin at 4°C or room temperature (samples for RNAscope). PFA-fixed tissues were washed in PBS and sectioned into 150 µm-to 300 µm-thick sections using a vibratome. Sections from the median or left lobes were used for analysis of clonal expansion during homeostasis and after CCl<sub>4</sub> injury. Additionally, sections from each of the left, median, right anterior, and right posterior lobe were used for analysis of clonal expansion during homeostasis in a subset of mice (Table S1). Sections from the right (anterior and posterior) lobe were used to analyze clonal expansion after AA injury because injury was more severe in this lobe. Sections from the median, left, or right anterior lobes were used to assess clone size in control mice 2–3 weeks after AAV injection. Vibratome sections were stained with rabbit anti-glutamine synthetase antibody at 1:2,000 dilution, which was detected with Alexa Fluor-647-conjugated donkey anti-rabbit antibody at 1:250 dilution. For 3D imaging, vibratome sections were cleared using a modified CUBIC protocol (Susaki et al., 2015; Susaki and Ueda, 2016) where incubation in Reagent 1A (10% weight Triton X-100, 5% weight N,N,N',N'-Tetrakis(2-hydroxypropyl)ethylenediamine, 10% weight urea, and 25 mM sodium chloride dissolved in ultrapure water) was done for 4 days to 1 week at 4°C, followed by staining with 1 µg/mL DAPI in a 1:1 solution of Reagent 2 (25% weight urea, 50% weight sucrose, 15% weight ultrapure water, and 10% weight triethanolamine):PBS overnight at 4°C, and incubation in Reagent 2 at room temperature for 3 hours to overnight. Cleared sections were mounted with Reagent 2 for imaging. In addition, fixed tissues were cryoprotected in 30% sucrose and embedded in OCT (Tissue-Tek) for cryosectioning. 7 µm-thick cryosections from *R26R<sup>tdRFP/ZG</sup>* mice were stained with rabbit anti-glutamine synthetase antibody and chicken anti-GFP antibody at 1:2,000 and 1:1,000 dilution, respectively, which were detected with Alexa Fluor-647-conjugated donkey anti-rabbit antibody and Alexa Fluor-488-conjugated donkey anti-chicken antibody, both at 1:250 dilution. In addition, these sections were stained with rabbit anti-DsRed antibody, chicken anti-GFP antibody, and mouse anti-glutamine synthetase antibody at 1:500, 1:1,000, and 1:1,000 dilution, respectively, which were detected with Alexa Fluor-555-conjugated donkey anti-rabbit antibody, Alexa Fluor-488-conjugated donkey anti-chicken antibody, and M.O.M. Immunodetection Kit with Alexa Fluor 647 streptavidin conjugate, all at 1:250 dilution. To assess Tert and *Axin2* expression in *R26R<sup>rb/wt</sup>* mice, 5 µm-thick sections of formalin-fixed paraffin-embedded livers were incubated with Tert or *Axin2* RNAscope probe and signal was amplified and detected with RNAscope 2.5 HD Reagent Kit-RED. Sections were subsequently incubated with rabbit anti-DsRed antibody at 1:25 dilution to detect mOrange-and mCherry-expressing clones. Anti-DsRed antibody signal was amplified by sequential incubation with donkey anti-rabbit biotin antibody and Alexa Fluor 647 streptavidin conjugate, both at 1:250 dilution. Endogenous biotin, biotin receptors, and streptavidin binding sites were blocked with Streptavidin/Biotin Blocking Kit. Sections of

formalin-fixed paraffin-embedded livers of C57/B6J mice were stained with rabbit anti-CCND1 antibody or mouse anti-PCNA antibody at 1:100 or 1:16,000 dilution, respectively, followed by 3,3'-Diaminobenzidine detection. Sections of formalin-fixed paraffin-embedded livers were used for H&E staining. Both immunohistochemistry and H&E staining were performed at Peninsula Histopathology Laboratory. Thick vibratome sections were imaged on a confocal microscope. Confocal image stacks were acquired with a step size of 4  $\mu\text{m}$  along the z axis. Thin cryosections and formalin-fixed paraffin-embedded liver sections were imaged on a fluorescence microscope or a confocal microscope. See Table S1 for numbers of fields imaged per sample. Fluorescent signal from each fluorophore was acquired separately, pseudo-colored, and the brightness and contrast optimized before combining into 1 RGB image using Fiji (Schindelin et al., 2012). Micrographs were prepared using Adobe Creative Suite and were cropped to focus on an area covering a representative half lobule containing 1 portal tract and 1 central vein, or to focus on a clone of interest. Exceptions are Figures S1A, S2A, S2B, and S2E–S2H, which were not cropped. Micrograph series featured in Video S1 were cropped to show a representative field or clone of interest.

**Replication, randomization and exclusion**—Experiments were replicated independently once (Figures 1F (9.5–9.7 and 13.6–13.7 months), 1G–1I, 2B, 2F, 2G, S1C, S1D, S1E–S1H (9.5–9.7 and 13.6–13.7 months), S1I–S1N, S2C, and S2I–S2N; Videos S1A, S1C–S1E, and S1G), twice (Figures 2C (6 x and 12 x CCl<sub>4</sub>), 2D (uninjured and AA), 2H, 2I, S1B (2–3 weeks), S2A, S2B, and S2D–S2H), or at least three times (Figures 1B, 1C–1E (time points > 1 year), 1F (2–3 weeks), 2A, 2C (3 x CCl<sub>4</sub>), 2D (1 x and 3 x CCl<sub>4</sub>), 2E, S1A, S1B (13.5–17 months), and S1E–S1H (2–3 weeks); Videos S1B and S1F). For each series of experiments, attempts at replication were successful. Mice excluded from the analysis shown in Figures 1 and S1 due to spontaneous development of liver pathologies are indicated in Table S1. Labeling efficiency with AAV8-TBG-Cre varied moderately with the virus production lot; an effort was made to inject the same lot into all mice within the same experiment. Extent of injury with AA showed variability between mice and within the same liver (Figure S2B); in Figures 2B, 2D, and S2D, analysis focused on fields that had autofluorescent cellular debris (2 of 11 mice were excluded because fields with cellular debris were not found in the sections analyzed). Mice from the same litter and sex were randomly assigned to different experimental conditions, and each condition had at least 1 male and 1 female mouse. Researchers were not blinded when analyzing results. No statistical methods were used to predetermine sample size.

## QUANTIFICATION AND STATISTICAL ANALYSIS

To generate the graphs in Figures 1F, S1E–S1H, S1J, S1K, and S2I, all 3D clones from 1–14 fields per sample were analyzed. Only clones completely within the tissue sample were analyzed. Number of cells per clone was determined based on clone morphology and nuclear staining with DAPI. Clones containing 2 mononucleated cells were distinguished from binucleated single-cell clones based on whether the cell shape appeared to be 2 cells and whether the 2 nuclei were separated by at least half a nuclear diameter or in separate planes. Hepatocyte hypertrophy was estimated from nuclear DAPI staining and cell size; a clone was considered hypertrophied if it had a nucleus or cell diameter at least 1/3 larger than neighboring hepatocytes in the same zone. Clones containing a cell located within 4

cell distances from the portal vein or bile duct were classified as periportal; clones containing a cell within 2 cell distances from the central vein were classified as pericentral; clones not meeting either criterion were classified as midlobular. Because the periportal and pericentral zones are smaller, clones were counted from additional fields to increase the number of clones in these zones. Number of new hepatocytes per 3D clone was calculated by subtracting the number of cells in each clone by 1, following the assumption that all clones are initially single cells. Dividing the total number of new hepatocytes by the number of 3D clones analyzed in each mouse or at each time point gives the average number of new hepatocytes per 3D clone as shown in Figures S1F and S1K and Table S1. To generate the graphs in Figures 2D and 2I, at least 3 fields were analyzed from 1 vibratome section of *R26R<sup>tb/wt</sup>* mice injected with high-or medium-dose AAV8-TBG-Cre and subjected to CCl<sub>4</sub> injury. 18–48 fields were analyzed from 1–7 vibratome sections of *R26R<sup>tb/wt</sup>* mice injected with low-dose AAV8-TBG-Cre and subjected to CCl<sub>4</sub> or AA injury. To generate the graphs in Figures 1H, 1I, S1M, and S1N, at least 10 10x fields of stained cryosectioned tissue were analyzed; each of the liver lobes of each mouse are represented in the fields analyzed. Hepatocytes were considered to be in the same 2D cluster if they shared a cell border. Clusters containing a cell located within 4 cell distances from the portal vein were classified as periportal, and clusters containing 1 glutamine synthetase-positive cell (usually within 2 cell distances from the central vein) were classified as pericentral; clusters not meeting either criterion were classified as midlobular. To account for differences in no-AAV cluster size across the lobule due to zonation of AAV8 transduction, cluster sizes were standardized by Z score calculated as  $Z = (x - \mu)/\sigma$  where  $x$  is the number of cells per 2D cluster and  $\mu$  and  $\sigma$  are the average and standard deviation, respectively, of the number of cells per no-AAV or AAV-Flp cluster in mice of the corresponding sex (Figures 1H and S1M) or in the corresponding lobular location in mice of the corresponding sex (Figures 1I and S1N) 2 weeks after AAV injection. To generate the graphs in Figures S2L and S2N, 3–6 fields were analyzed to assess *Tert* and *Axin2* expression in all hepatocytes; 76–108 fields were analyzed to assess *Tert* and 25–35 fields were analyzed to assess *Axin2* expression in lineage-traced clones.

Data were tabulated and analyzed in Microsoft Excel or GraphPad Prism. In Figures 1F, S1E, S1G, S1H, S1J, and S2I a similar number of clones were analyzed from each mouse within each group. Data from all mice in the group were pooled and Mann-Whitney U tests were used to compare different groups. Standardized Z score data from all mice in each group in Figures 1H, 1I, S1M, and S1N were pooled and Student's 2-sided unpaired t tests were used to compare different groups.  $\chi^2$  tests were used to determine goodness of fit to a Poisson distribution in Figure S1K. Student's 2-sided unpaired t tests or 2-sided unpaired t tests with Welch's correction were used to compare groups shown in Figures 2D, 2I, S1B, S1C, and S2N. A p value < 0.05 was considered statistically significant. Statistical parameters are shown in figures and figure legends. Error bars in the figures show SEM to illustrate how precisely the data define the mean; in the main text the mean  $\pm$  SD is given to show the variability. No methods were used to determine whether data met assumptions of statistical approach. Graphs were generated in Prism. In Figures 1F, 1H, 1I, S1E, S1G, S1H, S1M, and S1N width distribution of points is proportionate to the number of points at each y

axis value and represents data distribution. In Figures S1J and S2I minimizing overlap of individual data points is prioritized over representing shape of data distribution.

## Supplementary Material

Refer to Web version on PubMed Central for supplementary material.

## ACKNOWLEDGMENTS

F.C. was supported by NIH T32 DK060414 and the Jane Coffin Childs Memorial Fund for Medical Research, H.Y.L. by an Eli and Edythe Broad Regeneration Medicine and Stem Cell Fellowship, and H.W. by NIH R01 AA026578, CIRM DISC2-10088, and NIH P30 DK026743. The authors thank Donghui Wang (UCSF Preclinical Therapeutics Core) for tail vein injection, Tara Friedrich (UCSF Liver Center) and Jan Tchorz (Novartis) for discussion, and Pamela Derish (UCSF Department of Surgery) for manuscript editing.

## REFERENCES

- Alvarado TF, Puliga E, Preziosi M, Poddar M, Singh S, Columbano A, Nejak-Bowen K, and Monga SP (2016). Thyroid hormone receptor  $\beta$  agonist induces b-catenin-dependent hepatocyte proliferation in mice: implications in hepatic regeneration. *Gene Expr.* 17, 19–34. [PubMed: 27226410]
- Arrojo E Drigo R, Lev-Ram V, Tyagi S, Ramachandra R, Deerinck T, Bushong E, Phan S, Orphan V, Lechene C, Ellisman MH, and Hetzer MW (2019). Age mosaicism across multiple scales in adult tissues. *Cell Metab.* 30, 343–351.e3. [PubMed: 31178361]
- Bell P, Wang L, Gao G, Haskins ME, Tarantal AF, McCarter RJ, Zhu Y, Yu H, and Wilson JM (2011). Inverse zonation of hepatocyte transduction with AAV vectors between mice and non-human primates. *Mol. Genet. Metab* 104, 395–403. [PubMed: 21778099]
- Davidoff AM, Ng CY, Zhou J, Spence Y, and Nathwani AC (2003). Sex significantly influences transduction of murine liver by recombinant adeno-associated viral vectors through an androgen-dependent pathway. *Blood* 102, 480–488. [PubMed: 12637328]
- Duncan AW, Taylor MH, Hickey RD, Hanlon Newell AE, Lenzi ML, Olson SB, Finegold MJ, and Grompe M. (2010). The ploidy conveyor of mature hepatocytes as a source of genetic variation. *Nature* 467, 707–710. [PubMed: 20861837]
- Font-Burgada J, Shalpour S, Ramaswamy S, Hsueh B, Rossell D, Umemura A, Taniguchi K, Nakagawa H, Valasek MA, Ye L, et al. (2015). Hybrid periportal hepatocytes regenerate the injured liver without giving rise to cancer. *Cell* 162, 766–779. [PubMed: 26276631]
- Greig JA, Nordin JML, Draper C, McMenamin D, Chroscinski EA, Bell P, Gray JT, Richman LK, and Wilson JM (2018). Determining the minimally effective dose of a clinical candidate AAV vector in a mouse model of Crigler-Najjar syndrome. *Mol. Ther. Methods Clin. Dev* 10, 237–244. [PubMed: 30112420]
- Lin S, Nascimento EM, Gajera CR, Chen L, Neuhöfer P, Garbuzov A, Wang S, and Artandi SE (2018). Distributed hepatocytes expressing telomerase repopulate the liver in homeostasis and injury. *Nature* 556, 244–248. [PubMed: 29618815]
- Luche H, Weber O, Nageswara Rao T, Blum C, and Fehling HJ (2007). Faithful activation of an extra-bright red fluorescent protein in “knock-in” Cre reporter mice ideally suited for lineage tracing studies. *Eur. J. Immunol* 37, 43–53. [PubMed: 17171761]
- Minear S, Leucht P, Jiang J, Liu B, Zeng A, Fuerer C, Nusse R, and Helms JA (2010). Wnt proteins promote bone regeneration. *Sci. Transl. Med* 2, 29ra30.
- Miyaoka Y, Ebato K, Kato H, Arakawa S, Shimizu S, and Miyajima A. (2012). Hypertrophy and unconventional cell division of hepatocytes underlie liver regeneration. *Curr. Biol* 22, 1166–1175. [PubMed: 22658593]
- Red-Horse K, Ueno H, Weissman IL, and Krasnow MA (2010). Coronary arteries form by developmental reprogramming of venous cells. *Nature* 464, 549–553. [PubMed: 20336138]

- Sarin KY, Cheung P, Gilison D, Lee E, Tennen RI, Wang E, Artandi MK, Oro AE, and Artandi SE (2005). Conditional telomerase induction causes proliferation of hair follicle stem cells. *Nature* 436, 1048–1052. [PubMed: 16107853]
- Schaub JR, Huppert KA, Kurial SNT, Hsu BY, Cast AE, Donnelly B, Karns RA, Chen F, Rezvani M, Luu HY, et al. (2018). De novo formation of the biliary system by TGF $\beta$ -mediated hepatocyte trans differentiation. *Nature* 557, 247–251. [PubMed: 29720662]
- Schindelin J, Arganda-Carreras I, Frise E, Kaynig V, Longair M, Pietzsch T, Preibisch S, Rueden C, Saalfeld S, Schmid B, et al. (2012). Fiji: an open-source platform for biological-image analysis. *Nat. Methods* 9, 676–682. [PubMed: 22743772]
- Susaki EA, and Ueda HR (2016). Whole-body and whole-organ clearing and imaging techniques with single-cell resolution: toward organism-level systems biology in mammals. *Cell Chem. Biol* 23, 137–157. [PubMed: 26933741]
- Susaki EA, Tainaka K, Perrin D, Yukinaga H, Kuno A, and Ueda HR (2015). Advanced CUBIC protocols for whole-brain and whole-body clearing and imaging. *Nat. Protoc* 10, 1709–1727. [PubMed: 26448360]
- Wang B, Zhao L, Fish M, Logan CY, and Nusse R. (2015). Self-renewing diploid Axin2(+) cells fuel homeostatic renewal of the liver. *Nature* 524, 180–185. [PubMed: 26245375]
- Wilkinson PD, Delgado ER, Alencastro F, Leek MP, Roy N, Weirich MP, Stahl EC, Otero PA, Chen MI, Brown WK, and Duncan AW (2019). The polyploid state restricts hepatocyte proliferation and liver regeneration in mice. *Hepatology* 69, 1242–1258. [PubMed: 30244478]
- Yamamoto M, Shook NA, Kanisicak O, Yamamoto S, Wosczyzna MN, Camp JR, and Goldhamer DJ (2009). A multifunctional reporter mouse line for Cre-and FLP-dependent lineage analysis. *Genesis* 47, 107–114. [PubMed: 19165827]
- Yanger K, Knigin D, Zong Y, Maggs L, Gu G, Akiyama H, Pikarsky E, and Stanger BZ (2014). Adult hepatocytes are generated by self-duplication rather than stem cell differentiation. *Cell Stem Cell* 15, 340–349. [PubMed: 25130492]

**Highlights**

- Random lineage tracing provides a representative sample of all hepatocytes
- Liver homeostasis relies on modest proliferation of hepatocytes in all zones
- The burden of proliferation in liver regeneration is distributed among hepatocytes
- Chronic injury reveals differences in hepatocyte proliferation caused by ploidy

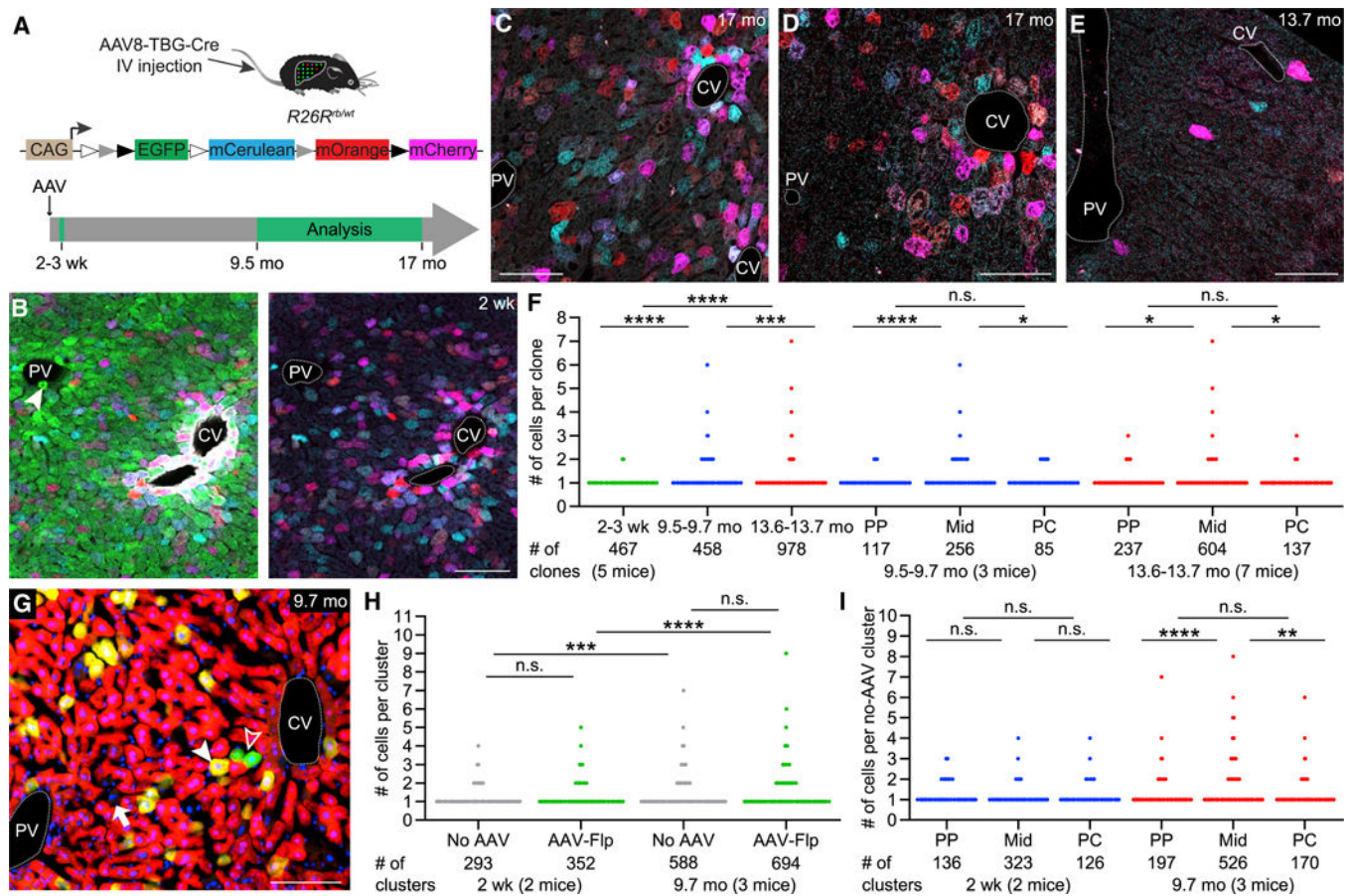


### Figure 1. Hepatocyte Proliferation in Liver Homeostasis

(A) Rosa26-Rainbow Cre reporter allele and lineage-tracing strategy. In the absence of Cre,  $R26R^{rb/wt}$  mice express EGFP in all cells. Hepatocyte-targeted AAV8-TBG-Cre mediates recombination at 1 set of the variant loxP sites, which deactivates EGFP and randomly activates mCerulean, mOrange, or mCherry expression. IV, intravenous; mo, months; wk, weeks; white triangle, loxN; gray triangle, lox2272; black triangle, loxP.

(B) Liver of a male  $R26R^{rb/wt}$  mouse 2 weeks after high-dose AAV8-TBG-Cre injection. Lineage-traced hepatocytes express mCerulean (light blue), mOrange (red), or mCherry (magenta) or a combination of these fluorophores. Hepatocytes and other liver cells not transduced by the AAV vector express only EGFP (green). Left image shows all 4 fluorophores; right image shows only the 3 Cre-activated fluorophores. Rare lineage-traced hepatocytes also express EGFP, presumably because 1 of the reporter alleles was not recombined. Portal tracts are identified by bile ducts (arrowhead) and pericentral hepatocytes by glutamine synthetase immunofluorescence (white). CV, central vein; PV, portal vein. Scale bar, 100 $\mu$ m.

(C–E) Livers of male  $R26R^{rb/wt}$  mice imaged at the indicated time points after high-dose (C), medium-dose (D), or low-dose (E) AAV8-TBG-Cre injection. Results are representative of 5–7 male and 4–6 female mice for each dose analyzed 9.5–17 months after AAV injection (Table S1). Scale bars, 100  $\mu$ m.

(F) Number of hepatocytes per 3D clone in male and female *R26R<sup>trb/wt</sup>* mice at the indicated time points after low-dose AAV8-TBG-Cre injection. 54–153 clones were analyzed in each mouse at 2 to 3 weeks, 142–167 clones at 9.5–9.7 months, and 103–181 clones at 13.6–13.7 months. PP, periportal; Mid, midlobular; PC, pericentral. Mann-Whitney U test; \*\*\*\*p < 0.0001; \*\*\*p < 0.001; \*p < 0.05; n.s., not significant.

(G) Liver of a female *R26R<sup>tdRFP/ZG</sup>* mouse 9.7 months after co-injection of AAV8-TBG-Cre and AAV9-TTR-Flp. AAV8-TBG-Cre-lineage-traced hepatocytes express tdRFP (red) and AAV9-TTR-Flp-lineage-traced hepatocytes express EGFP (green; open arrowhead). Hepatocytes transduced with both AAV vectors express tdRFP and EGFP and appear yellow in the merged image (closed arrowhead), whereas hepatocytes not transduced with either AAV vector express neither tdRFP nor EGFP and are identified by large nuclei (DAPI staining, blue; arrow). Scale bar, 100  $\mu$ m.

(H) Number of hepatocytes per 2D cluster not transduced with any AAV (no AAV) or transduced with AAV9-TTR-Flp (AAV-Flp) in 1 male and 1 female *R26R<sup>tdRFP/ZG</sup>* mouse 2 weeks and 1 male and 2 female mice 9.7 months after AAV8-TBG-Cre and AAV9-TTR-Flp co-injection. 99 and 194 no-AAV clusters and 117 and 235 AAV-Flp clusters were analyzed in male and female mice, respectively, at 2 weeks; 188–201 no-AAV and 206–275 AAV-Flp clusters were analyzed in each mouse at 9.7 months. Student's t test on standardized cluster size (see STAR Methods and Figure S1M); \*\*\*\*p < 0.0001; \*\*\*p < 0.001.

(I) Number of hepatocytes per not transduced 2D cluster in male and female *R26R<sup>tdRFP/ZG</sup>* mice 2 weeks and 9.7 months after AAV8-TBG-Cre and AAV9-TTR-Flp co-injection (same mice as in H). 220 and 365 clusters were analyzed in each mouse at 2 weeks; 201–466 clusters were analyzed in each mouse at 9.7 months. Student's t test on standardized cluster size (see STAR Methods and Figure S1N); \*\*\*\*p < 0.0001; \*\*p < 0.01.



(B) Liver of a female *R26R<sup>tb/wt</sup>* mouse injected with low-dose AAV8-TBG-Cre analyzed 2 weeks after 2 doses of AA. mCerulean and mOrange double-positive hepatocytes appear orange. Small white and magenta dots are autofluorescent cellular debris. Results are representative of 2 (1 male and 1 female) mice. Additional 3 (2 male and 1 female) mice analyzed 1 week after the last AA dose showed similar results (data not shown). Scale bars, 50  $\mu$ m.

(C) Livers of 3 male *R26R<sup>tb/wt</sup>* mice injected with high-dose AAV8-TBG-Cre analyzed 2 weeks after 3, 6, or 12 doses of CCl<sub>4</sub>. Results are representative of 5 (3 male and 2 female) mice for 3 doses and 2 (1 male and 1 female) mice each for 6 doses and 12 doses. Additional 3, 1, and 2 male and female mice analyzed 3–6 days after the last of 3, 6, and 12 doses of CCl<sub>4</sub> showed similar results (data not shown). Scale bars, 50  $\mu$ m.

(D) Left graph shows percentage of 3D clones with the indicated number of hepatocytes in 3 (1 male and 2 female) uninjured *R26R<sup>tb/wt</sup>* mice injected with low-dose AAV8-TBG-Cre (mice also shown in Figure 1F), 2 (1 male and 1 female) *R26R<sup>tb/wt</sup>* mice injected with low-dose and 1 female mouse injected with medium-dose AAV8-TBG-Cre, all injured with 1 dose of CCl<sub>4</sub>, and 3 (2 male and 1 female) *R26R<sup>tb/wt</sup>* mice injected with low-dose AAV8-TBG-Cre and injured with 2 doses of AA. Livers were analyzed 2 weeks after the single CCl<sub>4</sub> dose or 1 week after the last AA dose. 46–99 clones from the midlobular zone and 21–69 clones each from the periportal and pericentral zones were analyzed in each mouse. Right graph shows percentage of 3D clones with the indicated number of hepatocytes in 8 (4 male and 4 female) *R26R<sup>tb/wt</sup>* mice injected with high-dose AAV8-TBG-Cre analyzed 4–6 days or 2 weeks after 3 doses of CCl<sub>4</sub>. 76–180 clones from the midlobular zone and 32–102 clones each from the periportal and pericentral zones were analyzed in each mouse. In mice receiving AA, liver lobules lacking injured portal areas were excluded from analysis (see STAR Methods). Results are means + SEM. Student's t test; \*\*\*p < 0.001; \*\*p < 0.01; \*p < 0.05. Differences between 1-, 2-, and 3-cell clones in periportal and pericentral zones are indicated by p values above bars.

(E) Characteristic types of hepatocyte clones in a male *R26R<sup>tb/wt</sup>* mouse injected with high-dose AAV8-TBG-Cre analyzed 4 days after 3 doses of CCl<sub>4</sub>, including single large (hypertrophied) binucleated hepatocytes, hepatocytes that divided once and generated 2-cell clones, or hepatocytes that proliferated more than once, generating 3 cells that either streamed along the portal to central axis or formed a nodule. Nuclei are identified by DAPI staining (white). Results are representative of 2 (1 male and 1 female) mice. Scale bars, 50  $\mu$ m.

(F) mCherry (magenta)-expressing clone consisting of several small hepatocytes with small nuclei and 2 large hepatocytes with large nuclei in a male *R26R<sup>tb/wt</sup>* mouse injected with low-dose AAV8-TBG-Cre analyzed 3 days after 6 doses of CCl<sub>4</sub>. Nuclei are identified by DAPI staining (white). Scale bar, 50  $\mu$ m.

(G) mCherry (magenta)-expressing clone consisting of many small hepatocytes that covers the distance from the portal vein to the central vein in a female *R26R<sup>tb/wt</sup>* mouse injected with high-dose AAV8-TBG-Cre analyzed 4 days after 12 doses of CCl<sub>4</sub>. Adjacent to this clone is an mCerulean (light blue)-expressing 1-cell clone consisting of a large hepatocyte stretching along the portal to central axis. Nuclei are identified by DAPI staining (white). Scale bar, 50  $\mu$ m.

(H) Columns of small images show the fluorophores mCerulean (light blue), mOrange (red), mCherry (magenta), and EGFP (green) separately; large images show them merged. Left column and related merged image show hepatocytes in a male  $R26R^{tb/wt}$  mouse 2 weeks after high-dose AAV8-TBG-Cre injection before initiation of liver injury. Many hepatocytes express more than 1 fluorophore, i.e., are polyploid. Scale bar, 25  $\mu\text{m}$ . Right column and related merged image show hepatocyte clones in a male  $R26R^{tb/wt}$  mouse injected with high-dose AAV8-TBG-Cre analyzed 4 days after 12 doses of CCl<sub>4</sub>. Many large clones consist of diploid hepatocytes as indicated by expression of only 1 fluorophore. Scale bar, 50  $\mu\text{m}$ .

(I) Percentages of diploid-enriched (1 color) and polyploid (>1 color) hepatocyte clones in 4 (2 male and 2 female)  $R26R^{tb/wt}$  mice analyzed 2 weeks after high-dose AAV8-TBG-Cre injection and in 4 (2 male and 2 female)  $R26R^{tb/wt}$  mice injected with high-dose AAV8-TBG-Cre analyzed 4 days or 2 weeks after 12 doses of CCl<sub>4</sub>. In injured mice, only large clones consisting of  $\geq 12$  cells were analyzed. Results are means + SEM. Welch's t test; \*\*p < 0.01. Differences between 1 color and >1 color in pericentral and periportal zones are indicated by p values above bars.

## KEY RESOURCES TABLE

REAGENT or RESOURCE	SOURCE	IDENTIFIER
<b>Antibodies</b>		
Mouse monoclonal anti-glutamine synthetase	BD Transduction Laboratories	Cat# 610517; RRID AB_397879
Mouse monoclonal anti-PCNA	Cell Signaling	Cat# 2586; RRID AB_2160343
Chicken polyclonal anti-GFP	Abcam	Cat# ab13970; RRID AB_300798
Donkey polyclonal anti-Chicken IgY, Alexa Fluor 488	Jackson ImmunoResearch	Cat# 703-545-155; RRID AB_2340375
Donkey polyclonal anti-Rabbit IgG, Biotin	Jackson ImmunoResearch	Cat# 711-065-152; RRID AB_2340593
Donkey polyclonal anti-Rabbit IgG, Alexa Fluor 555	Thermo Fisher Scientific	Cat# A-31572; RRID AB_162543
Donkey polyclonal anti-Rabbit IgG, Alexa Fluor 647	Thermo Fisher Scientific	Cat# A-31573; RRID AB_2536183
Rabbit monoclonal anti-CCND1	Thermo Fisher Scientific	Cat# MA5-14512; RRID AB_10985779
Rabbit polyclonal anti-DsRed	Takara Bio	Cat# 632496; RRID AB_10013483
Rabbit polyclonal anti-glutamine synthetase	Abcam	Cat# ab49873; RRID AB_880241
<b>Bacterial and Virus Strains</b>		
AAV8-TBG-Cre	Penn Vector Core	AV-8-PV1091
AAV9-TTR-Flp	Vector Biolabs	Custom order
<b>Chemicals, Peptides, and Recombinant Proteins</b>		
Allyl alcohol	Sigma-Aldrich	Cat# 240532
Carbon tetrachloride	Sigma-Aldrich	Cat# 319961
N,N,N',N'-Tetrakis(2-hydroxypropyl)ethylenediamine	Tokyo Chemical Industry (TCI)	Cat# T0781
Paraformaldehyde	VWR International	Cat# 100504-858
D-Sorbitol	Sigma-Aldrich	Cat# S1876
Triethanolamine	Sigma-Aldrich	Cat# 90279
Triton X-100	Sigma-Aldrich	Cat# X100
Urea	Thermo Fisher Scientific	Cat# 15505035
<b>Critical Commercial Assays</b>		
H&E and immunohistochemical stainings	Peninsula Histopathology Laboratory	N/A
M.O.M. Immunodetection Kit	Vector Laboratories	Cat# BMK-2202
RNAscope 2.5 HD Reagent Kit-RED	Advanced Cell Diagnostics (ACD)	Cat# 322350
RNAscope Probe-Mm-Axin2	Advanced Cell Diagnostics (ACD)	Cat# 400331
RNAscope Probe-Mm-Tert	Advanced Cell Diagnostics (ACD)	Cat# 313441
Streptavidin, Alexa Fluor 647	Thermo Fisher Scientific	Cat# S21374
Streptavidin/Biotin Blocking Kit	Vector Laboratories	Cat# SP-2002
<b>Experimental Models: Organisms/Strains</b>		
<i>R26R<sup>tr/b</sup></i> mice	Red-Horse et al., 2010	N/A
<i>R26R<sup>tdRFP/tdRFP</sup></i> mice	Luche et al., 2007	N/A
<i>R26R<sup>ZG/ZG</sup></i> mice	Schaub et al., 2018	N/A
C57BL/6J mice	Jackson Laboratory	Stock# 000664

REAGENT or RESOURCE	SOURCE	IDENTIFIER
Software and Algorithms		
Creative Suite	Adobe	CC 2017
Excel	Microsoft	Office 16
Fiji	Schindelin et al., 2012	N/A
Prism	GraphPad	Version 8.1.2
Other		
BX51 fluorescence microscope	Olympus	N/A
TCS SP5 confocal microscope	Leica	N/A
VT1000 S vibrating-blade microtome	Leica	Cat# 14047235613

Author Manuscript

Author Manuscript

Author Manuscript

Author Manuscript